What are the causes of tropical cirrus longwave biases in global storm-resolving simulations?

R.L. Atlas[1], C.S. Bretherton[2], A.B. Sokol[1], P.N. Blossey[1], M.F. Khairoutdinov[3]

[1]Dept. of Atmospheric Sciences, University of Washington, Seattle, WA
[2]Allen Institute for Artificial Intelligence, Seattle, WA
[3]School of Marine and Atmospheric Sciences, Stony Brook University, Stony Brook, NY
[1]3920 Okanogan Ln, Seattle, WA 98195
[2]2157 N Northlake Way #110, Seattle, WA 98103
[3]Endeavour, 145, Stony Brook, NY 11790

Key Points:

- Global storm-resolving models are uniquely suited for microphysics sensitivity studies.
- Mean tropical longwave CRE biases vary over 20 W m^{-2} and cirrus coverage varies over a factor of two depending on microphysics.
- Efficiency of cloud ice sublimation and conversion to snow, and limiters on cloud ice number affect simulated cirrus.

Corresponding author: Rachel Atlas, `ratlas@uw.edu`

Abstract

Cirrus control the longwave radiative budget of the tropics. For the first time, we quantify the variability in cirrus properties and longwave cloud radiative effects (CREs) that arises from using different bulk ice microphysical parameterizations within a single global storm-resolving model. We run five-day meteorologically-nudged simulations with four commonly-used microphysics schemes (M2005, Thompson, P3 and SAM1MOM) and evaluate them with satellite products and in situ observations. Tropical average longwave CRE varies over 20 W m^{-2} between schemes. Within the Thompson scheme, rapid autoconversion of cloud ice to snow leads to deficient anvil cirrus even with radiatively active snow. SAM1MOM, which uses saturation adjustment for cloud ice, also has deficient anvil cirrus. M2005 and P3 simulate cirrus with realistic frozen water path, and P3 best reproduces observed longwave CRE. Even in those schemes, ice crystal number concentrations commonly hit limiters and lack the observed variability and dependence on frozen water content.

Plain Language Summary

Recently, advancements in computing capabilities have made it possible for atmospheric scientists to simulate Earth's global atmosphere with higher resolution than ever before. This new generation of models, called global-storm resolving models, have a horizontal resolution of just a few kilometers, which is adequate to resolve thunderstorms. As a result, they simulate clouds more realistically than traditionally climate and weather models and are a great tool for diagnosing cloud biases in atmospheric models. Here, we run a single global storm-resolving model with four different representations of cloud physics called M2005, P3, SAM1MOM and Thompson. We evaluate simulated tropical cirrus clouds, which are stratiform ice clouds at the top of the troposphere that reduce the amount of infrared radiation emitted by the Earth, with satellite data to see which representations have the best performance. We find that tropical cirrus cloud coverage varies over a factor of two across the different representations, leading to differences in the amounts of infrared radiation emitted by the Earth. SAM1MOM and Thompson make two few cirrus clouds causing too much infrared radiation to be emitted, M2005 makes slightly too many cirrus causing too little infrared radiation to be emitted, and P3 makes about the right amount.

1 Introduction

Anvil cirrus, which flow outward from deep convective cores (Deng et al., 2016), reflect solar radiation and absorb longwave radiation from Earth's surface and re-emit it at colder temperatures, thereby reducing outgoing longwave radiation and heating the atmosphere (Hartmann et al., 2001). Atmospheric models must adequately represent the formation, evolution and optical properties of anvil cirrus to reproduce the observed radiative budget of the tropics.

Anvil cirrus are sensitive to the representation of deep convection and ice microphysics. These influences are difficult to disentangle in coarse resolution global models, where both are parameterized. Global storm-resolving models, which typically have sub-5 km horizontal grid spacing and explicit rather than parameterized deep convection, provide a unique opportunity to study how ice microphysics alone influences the representation of anvil cirrus.

Nugent et al. (2022) and Turbeville et al. (2022) studied the representation of tropical deep convection, cirrus and top-of-atmosphere radiation across the set of global storm-resolving models participating in the DYnamics of the Atmospheric general circulation Modeled On Non-hydrostatic Domains (DYAMOND) project. Here, we take a complementary approach, isolating the sensitivity of anvil cirrus to ice microphysics by running one such model with four different microphysics schemes. Sullivan and Voigt (2021) used regional storm-resolving simulations to show that the representation of ice microphysics exerted strong control over the radiative budget of the Asian monsoon region. We extend their findings to the entire tropics and identify additional microphysical constraints on anvil cirrus properties.

2 Data

Four five-day global storm-resolving simulations are run with the Global System for Atmospheric Modelling (Khairoutdinov et al., 2022). They are set up identically, as described in Atlas et al. (2022), except that they are run with different bulk microphysics schemes: M2005 (Morrison et al., 2005), Thompson (Thompson et al., 2008), P3 (Morrison & Milbrandt, 2015) with one ice class, and SAM1MOM (Khairoutdinov & Randall, 2003). The differences between the schemes in their parameterizations of ice processes are summarized in Text S1. The simulations have approximately 4 km horizontal resolution in

the tropics and about 500 m vertical resolution between 5 and 19 km. They are initialized from ERA5 reanalysis (Hersbach et al., 2020) at 00 UTC 16 Feb. 2018. We analyze days 2-5 of the simulations (17-20 February 2018) throughout this study, allowing one day for model spinup, long enough for cloud statistics to equilibrate (?, ?). Simulated temperature and horizontal winds (but not humidity or clouds) are nudged to ERA5 reanalysis with a damping timescale of 24 hours. This nudging strategy ensures that the model output can faithfully be compared with coincident real-world observations and that differences between simulated clouds can primarily be attributed to the bulk microphysics schemes.

Simulated longwave and shortwave cloud radiative effects (CREs) are compared with coincident retrievals from Clouds and the Earth's Radiant Energy System level 3 data (Doelling et al., 2013; NASA/LARC/SD/ASDC, 2017), referred to hereafter as CERES. CERES has hourly temporal resolution and $1° \times 1°$ horizontal resolution.

Retrieved frozen water content (FWC) and effective radii (r_e) from the DARDAR-CLOUD dataset (Delanoë & Hogan, 2010) versions V2.1.0 and V3.10 (Cazenave et al., 2019) and the Cloudsat and CALIPSO Ice Cloud Property Product (2C-ICE) (Deng et al., 2015) version RF05 are used to evaluate simulated anvil cirrus microphysics and macrophysics. These retrievals have a horizontal resolution of 1.4 km, comparable to that of the simulations. The vertical resolution of DARDAR and 2C-ICE are 60 m and 240 m, respectively. We use data from the Februaries of 2007-2012.

Simulated microphysics are evaluated with in situ airborne observations of ice crystal number concentration and FWC (Krämer, Rolf, Spelten, Afchine, et al., 2020; Krämer, Rolf, & Spelten, 2020). We hereafter refer to this dataset as the 'Microphysics Guide'. Text S2-S3 and Figures S1-S3 further discuss our use of DARDAR, 2C-ICE and the Microphysics Guide.

3 Microphysics schemes exhibit wide-ranging tropical longwave cloud radiative effects

Figure 1 compares simulated CREs with CERES. Throughout this study, radiative fluxes are defined as positive downwards, so that negative CREs indicate energy lost from the Earth. Shortwave CRE biases (panel b) are largest and most scheme-dependent over the Southern Ocean, as discussed in Atlas et al. (2022); these are sensitive to all clouds,

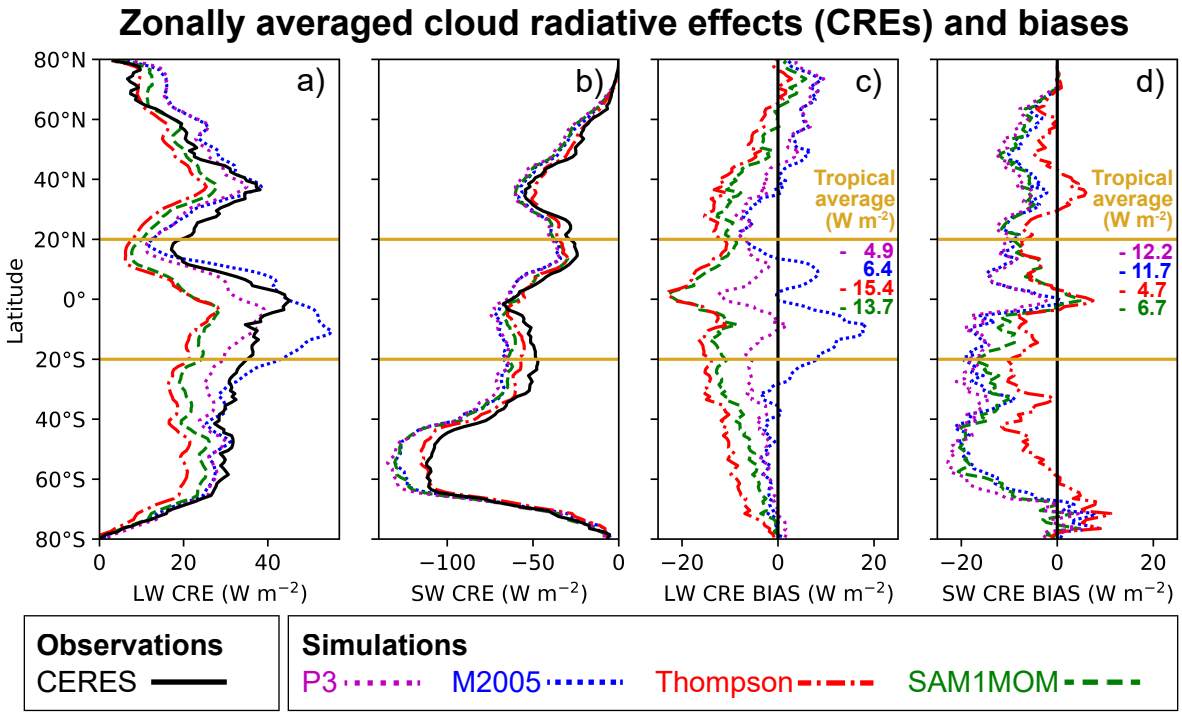

Figure 1. (a-b) Zonal average top of atmosphere CREs and (c-d) their biases vs. CERES. Yellow lines delineate the tropical analysis region (20°S - 20°N).

but especially to marine boundary layer clouds because of their extensive coverage and substantial albedo. In this study, however, we focus on the region between the yellow parallel lines at 20°N and 20°S, hereafter referred to as 'the tropics'. This is a region of strong sensitivity of longwave CRE, produced mainly by cirrus clouds, to the microphysics scheme (panel a).

Longwave and shortwave CRE biases for the four schemes are plotted on panels c-d. Their area-weighted tropical means (printed on the plots) vary over ranges of 7.5 and 22 W m^{-2}, respectively. While all simulations are too bright in the shortwave, the sign of the longwave CRE bias differs between M2005, whose clouds have excessive longwave CRE, and the other schemes. M2005 and P3 have smaller average longwave CRE biases than SAM1MOM and Thompson.

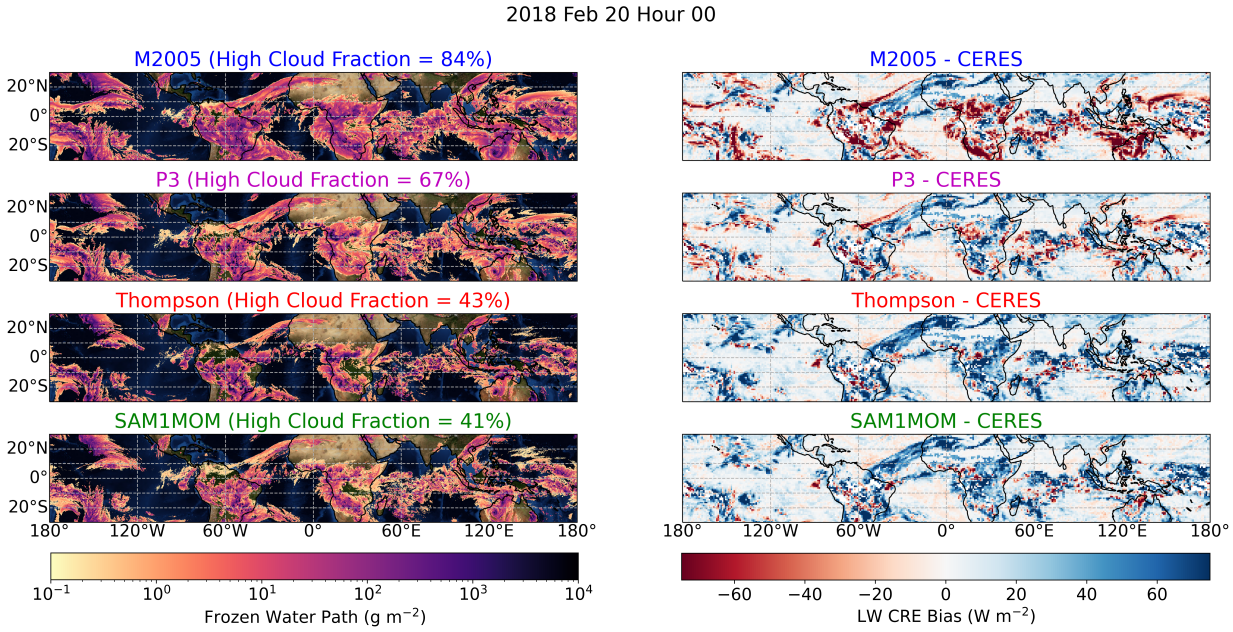

Figure 2. **left:** Snapshots of simulated FWP for columns with CTH > 10 km on the simulations' native grid. **right:** Coincident snapshots of longwave CRE bias compared to CERES on a coarsened 1° x 1° grid.

4 Variability in anvil cirrus coverage and optical properties lead to diverse longwave cloud radiative effects

Figure 2 shows coincident snapshots at an arbitrarily-chosen time of simulated frozen water path (FWP, the sum of the cloud ice, snow and graupel water paths) for columns containing high cloud, on the left, and biases in simulated longwave CRE coarsened to a 1°x1° grid, on the right. Cloud top height (CTH) is defined as the highest model level with FWC (the sum of the cloud ice, snow and graupel water contents) $> 10^{-4}$ g m^{-3} (the limit of lidar detectability as discussed in Text S2). Columns are identified as containing high cloud if they have CTH $\geq$ 10 km. The fraction of columns within the mapped area that meet these criteria is listed in the title of each snapshot. The coarsened longwave CRE bias is sensitive to both cloud fraction and cloud radiative properties. Animation S1 loops through versions of Figure 2 for each of the 96 hours of model output within days 2-5 of the simulations, showing that each hourly snapshot is representative of the entire four day period.

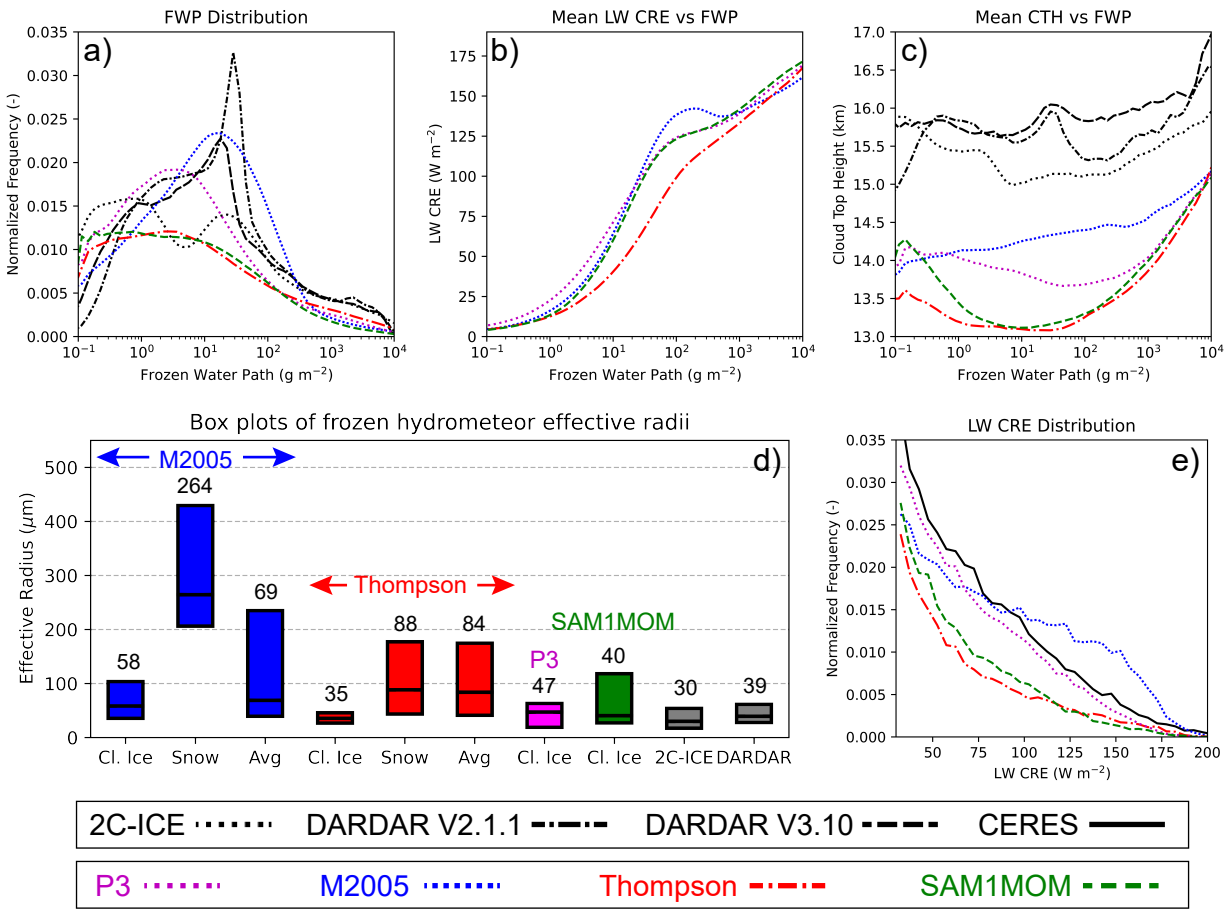

Figure 3. Tropical nighttime: **a)** PDF of FWP **b)** Mean longwave CRE, and **c)** Mean CTH, both as binned by FWP. **d)** Box plots with medians (black lines and numbers printed above each box) of frozen hydrometeor r_e. **e)** PDF of longwave CRE for 1° x 1° boxes. Only columns with CTH > 10 km and grid cells with FWC > 10^{-4} g m^{-3} are used in panels **a-d**.

M2005 has the largest high cloud fraction and extensive areas of negative longwave cloud biases, associated with deep convection (FWP > 10^3 g m^{-2}) and anvil cirrus (10 $\leq$ FWP $\leq$ 10^3 g m^{-2}). Thompson and SAM1MOM have half of M2005's cloud fraction and positive longwave biases in most areas of anvil cirrus. P3's high cloud fraction lies between that of M2005 and Thompson/SAM1MOM. With a mixture of positive and negative biases associated with anvil cirrus, P3 has the fewest areas with large biases of either sign.

Figure 3 statistically summarizes relationships between high cloud properties and longwave cloud biases, using CERES, DARDAR and 2C-ICE to provide observational

constraints on the simulations. The CALIPSO lidar used by DARDAR and 2C-ICE has greater sensitivity at night, during which it can detect FWCs $\geq 10^{-4}$ g m^{-3} (Text S2). Thus, we use DARDAR and 2C-ICE data from the nighttime A-train overpass, which crosses the equator at approximately 1:30 AM local time. For consistency, we also sample CERES and the simulations at night. FWCs $< 10^{-4}$ g m^{-3} are filtered out of the simulations and satellite retrievals.

In Figure 3a, we evaluate distributions of simulated FWP from columns containing high cloud (CTH $>$ 10 km) using DARDAR and 2C-ICE. The simulations and the two DARDAR datasets have unimodal distributions of FWP whereas 2C-ICE has a bimodal distribution. The discrepancy between DARDAR and 2C-ICE for FWPs $<$ 30 g m^{-3}, noted by Hong et al. (2016), emphasizes limitations on constraining FWP from CALIPSO in tropical cirrus too thin to be detected by CloudSat. For FWPs between 30 g m^{-2} and 300 g m^{-2}, M2005 and P3 bracket the observations, with P3 slightly underestimating anvil cirrus coverage, and M2005 slightly overestimating it. SAM1MOM and Thompson starkly underestimate anvil cirrus coverage. Satellite retrievals from deep convective cores (FWPs $> 10^3$ g m^{-2}) are uncertain (Delanoë & Hogan, 2010) so the apparent low FWP bias of the simulations may not be concerning.

Figure 3b shows mean longwave CRE as a function of FWP for the simulations, at the model 4 km grid resolution. M2005 has the strongest longwave CRE for FWPs between 10 and 10^3 g m^{-2}, and Thompson has the weakest.

Variability in longwave CRE for a fixed FWP can be caused by differences in cloud top temperature. In the tropics, cloud top temperature is tightly linked to CTH. Figure 3c shows mean CTH as a function of FWP for the simulations and the satellite retrievals. CTH is biased low in all simulations as explained later in this section. M2005 has the highest CTH for FWPs $>$ 1 g m^{-2}, which contributes to its stronger longwave CRE in Figure 3b. However, CTH does not explain the differences in Figure 3b between SAM1MOM, Thompson and P3.

Differences between the simulated longwave CRE in Figure 3b could also come from differences in effective radii (r_e). Figure 3d shows box plots of r_e of frozen hydrometeors for the simulations, 2C-ICE and DARDAR V3.10 (the two versions of DARDAR have similar r_e). For M2005 and Thompson, $r_{e,avg}$ is an optical depth preserving average of the cloud ice and snow effective radii, $r_{e,i}$ and $r_{e,s}$, which is directly comparable to satellite-

retrieved r_e. For P3, there is only one frozen hydrometeor class and for SAM1MOM, only cloud ice is radiatively active, so the snow contribution to r_e is neglected.

In M2005, the median $r_{e,avg}$ is similar to the median $r_{e,i}$ because cloud ice dominates the frozen hydrometeor mass (Figure 3d). In Thompson, the median $r_{e,avg}$ is similar to the median $r_{e,s}$ because snow dominates the frozen hydrometeor mass. This causes Thompson to have an unrealistically large $r_{e,avg}$, which contributes to it having the weakest longwave CRE in Figure 3b. All simulations have larger average median r_e than observed, consistent with Stanford et al. (2017).

Figure 3e shows the tail of the histogram of 1° x 1° nighttime longwave CRE for the four simulations and for CERES, which includes areas that contribute most to the tropical average and to differences between simulations and CERES. M2005 has too many areas with average longwave CRE > 100 W m^{-2} because it has more anvil cirrus than DARDAR and 2C-ICE (Figure 3a). Thompson and SAM1MOM have too few areas with average longwave CRE > 30 W m^{-2}, due to deficient anvil cirrus and (for Thompson) unrealistically large r_e.

Figure 4 compares simulated vertical profiles of thermodynamic and cloud properties with two ERA5 datasets, DARDAR and 2C-ICE. Figure 4a shows temperature profiles from ERA5 on 37 pressure levels and 137 model levels. In all simulations, temperature was nudged to pressure-level data (black dots), linearly interpolated to the gSAM model levels. The ERA5 model level data (black line) better resolves the 16-18 km layer, which includes the cold point at 17.3 km. All simulations have a warm bias in that layer and a cold point near 16 km instead of 17.3 km.

Figure 4b show profiles of average relative humidity with respect to ice (RH_i). SAM1MOM has a lower average RH_i than the other simulations and ERA5, particularly above 14 km, possibly because it uses saturation adjustment for cloud ice, preventing RH_i from ever exceeding 100%. The other simulations have higher RH_i than ERA5 near the cold point, but ERA5 may be biased by its internal ice microphysical modeling assumptions in the tropical tropopause layer, where routine observations of the very low water vapor concentration are uncertain.

Figure 4c shows profiles of cloud fraction. For all simulations, the altitudes of maximum cloud fraction are 2 km lower than observed, likely due to their artificially low-

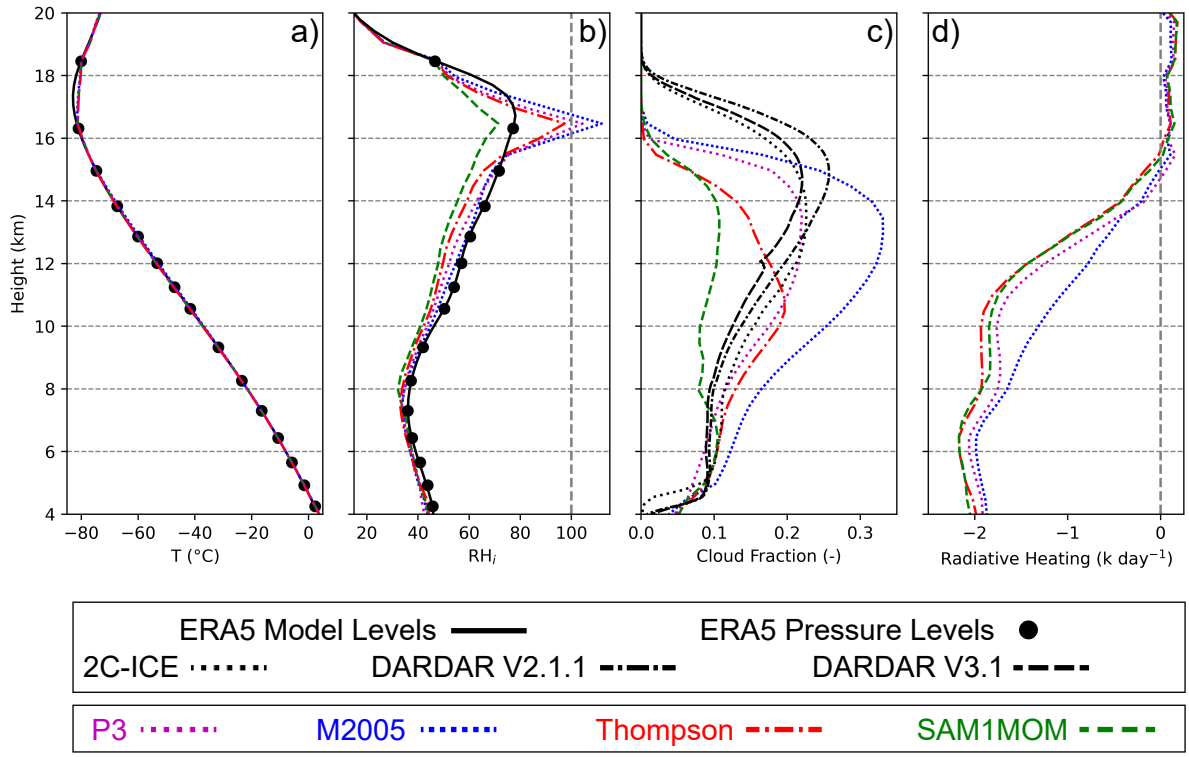

Figure 4. Vertical profiles of tropical nighttime-mean **a)** temperature, **b)** RH_i, **c)** cloud fraction (FWC $> 10^{-4}$ g m^{-3} only), and **d)** longwave radiative cooling.

ered cold point altitude. Below 14.5 km, P3 agrees well with both DARDAR datasets and 2C-ICE, M2005 overestimates cloud fraction, and SAM1MOM and Thompson underestimate it. In M2005 and P3, cloud fraction increases monotonically up to the base of the tropical tropopause layer at 14 km. Thompson's peak cloud fraction is only at 10.5 km, likely due to excessively efficient conversion of cloud ice to quickly falling snow. SAM1MOM has a nearly constant cloud fraction throughout the troposphere.

Figure 4d shows longwave radiative cooling profiles for the simulations. Cirrus clouds reduce radiative cooling by absorbing upwelling longwave radiation. M2005 has up to 0.5 K day^{-1} less radiative cooling than the other simulations between 8 and 13 km due to its comparably large cirrus coverage. Thompson and SAM1MOM, which have the smallest cirrus coverage, correspondingly have the strongest longwave cooling. These results are consistent with the findings of Hu et al. (2021).

Longwave CRE biases in the simulations can largely be explained by biases in the amount, the vertical structure, and the r_e of anvil cirrus, all of which can be estimated from spaceborne lidar and radar. These biases depend on the microphysics scheme; overall P3 best matches remote-sensing observations, followed by M2005, with Thompson and SAM1MOM producing far too little tropical cirrus.

5 Simulated ice crystal populations lack observed variability

As a complementary test of the microphysics schemes, we compare simulated ice crystal number concentration (N_{ice}) and FWC with in situ airborne observations from several tropical field studies, synthesized in the Microphysics Guide (see Text S3 and Figure S3), which have been coarsened to 0.04 Hz to match the horizontal resolution of the simulations. All observational data is from heights above 10 km, and latitudes between 20°S and 20°N; model histograms are accumulated from all post-spin-up output times (day and night) at all tropical high-cloud grid points.

Figure 5 shows 2D histograms of FWC and N_{ice} for M2005, P3, Thompson and in situ observations. SAM1MOM is omitted because it does not predict N_{ice} for any hydrometeor classes. N_{ice} and FWC for M2005 and Thompson include cloud ice, graupel and snow. Vertical lines overlaid on the 2D histograms show limiters specified within the microphysics schemes. These limiters are designed to prevent algorithms within the schemes from producing physically implausible results; if the limiter is frequently active, this sug-

gests problems with parameterization assumptions made within the scheme. Dotted lines show limiters on total cloud ice concentration and dashed lines show limiters on the concentration of ice particles produced through deposition nucleation, which is the dominant mode of nucleation within the temperature range investigated here. In Thompson, the two limiters are the same.

In M2005 and P3, most grid cells have values of N_{ice} that are very close to the smaller of these two limiters, which are 0.3 and 0.1 cm^{-3}, respectively. They have higher mean N_{ice} than the in situ observations and lack the observed variability in N_{ice} and dependence of N_{ice} on FWC. In the 2D histogram for P3, the grid cells between the two limiter values, which primarily have high FWCs, have experienced homogeneous freezing of cloud droplets. There is no homogeneous freezing of aerosol in any microphysics schemes used here. Thompson has many grid cells with tiny FWC and N_{ice} and a subpopulation of grid cells dominated by snow (a large ratio of FWC to N_{ice}) as a result of efficiently converting most cloud ice to snow. Although P3 lacks the observed variability, its mean N_{ice} is closest to the observed mean.

6 Conclusions

Tropical longwave cloud radiative effects (CREs) simulated by a global storm-resolving model are sensitive to ice microphysics. Average biases in longwave CRE vary over a 22 W m^{-2} range across four simulations which differ only in their microphysical schemes, due to variability in cirrus amount, thickness, cloud top height, and ice crystal number and size.

Simulations run with Thompson and SAM1MOM microphysics had very weak longwave CREs. The Thompson scheme quickly converts cloud ice to larger snow particles, which fall quickly and reduce cirrus cloud cover, and decrease the optical depth of the remaining cirrus, even though the snow is radiatively active. SAM1MOM's small cirrus coverage may be related to the instantaneous sublimation of sedimenting cloud ice in subsaturated conditions.

The other two simulations, run with M2005 and P3 microphysics, had stronger longwave CREs which agreed better with satellite observations. M2005's cirrus coverage is larger than observed, causing it to overestimate longwave CRE. P3's cirrus coverage is slightly smaller than observed, causing a slight underestimation of longwave CRE. Sim-

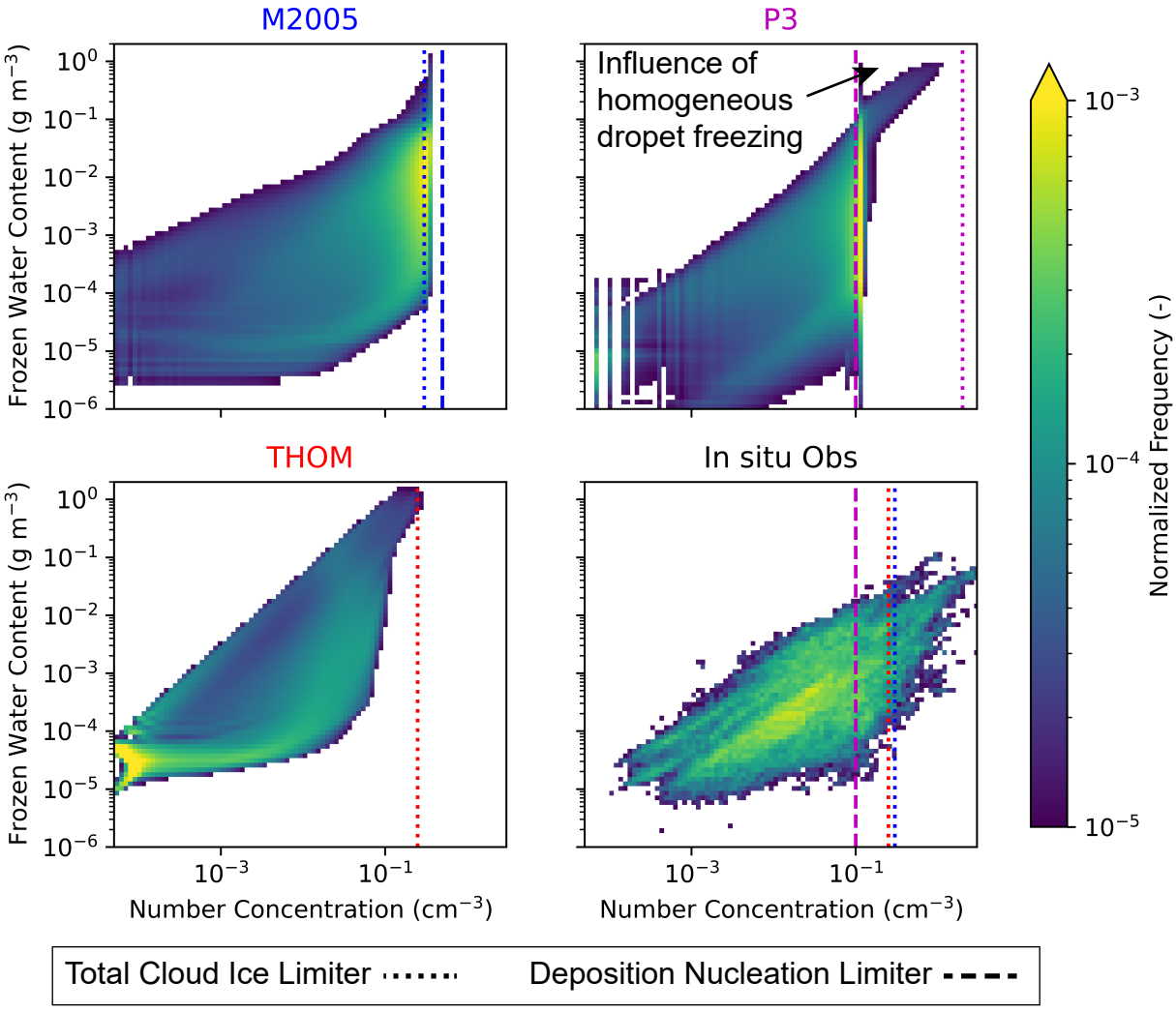

Figure 5. 2D histograms of FWC (on the y-axis) and N_{ice} (on the x-axis). Dashed and dotted lines indicate limiters on total cloud ice number concentration and cloud ice particles that can be formed through deposition nucleation, respectively.

ulated ice crystal number concentrations in M2005 and P3 ubiquitously hit arbitrary limiters within the microphysics schemes. As a result, typical ice crystal number concentrations lack the observed variability and dependence on frozen water content. P3 limits its ice concentrations to be a factor of three lower than M2005; this discrepancy may account for most of their differences in anvil cirrus coverage and thickness. Overall, P3 performed most skillfully of the four tested schemes across our diverse suite of observational comparisons.

Our results may have some sensitivity to model setup and forcing. The gSAM DYAMOND simulation, run with SAM1MOM, agreed considerably better with observations in regional analyses of the tropics (Nugent et al., 2022; Turbeville et al., 2022) than the SAM1MOM simulation evaluated here. DYAMOND was free-running rather than nudged, in boreal summer rather than austral summer, and used a slightly different tuning of SAM1MOM. While the relative differences between microphysical parameterizations are likely insensitive to these configuration differences, they could have a larger effect on the observational comparisons. We recommend further study of this important issue.

Adequately representing tropical convectively initiated cirrus is necessary for constraining tropical longwave CREs in global atmospheric models. Global storm-resolving models, which resolve deep convection, provide a unique opportunity to examine the sensitivities of anvil cirrus to the choice of ice microphysics scheme and identify important control parameters within schemes. We find that overly efficient autoconversion of cloud ice to snow causes deficient anvil cirrus. Tropical cirrus ice crystal formation and loss mechanisms need to be more realistically represented (a challenge), so that ice crystal number concentrations are not overly controlled by arbitrary limiters. While we focus on tropical cirrus here, global storm-resolving models have great potential for evaluating and improving the microphysical representation of clouds and precipitation across all climate regimes.

7 Open Research

CERES(NASA/LARC/SD/ASDC, 2017), 2C-ICE R05 (`https://www.cloudsat.cira.colostate.edu/data-products/2c-ice`), DARDAR-CLOUD V2.1.0 and V3.10 (`http://www.icare.univ-lille1.fr`), and the Microphysics Guide (Krämer, Rolf, & Spelten, 2020) are publicly available online. Simulated model output cannot be made

available due to the experimental nature of the simulations and the large storage space required.

Acknowledgments

We acknowledge funding from U.S. National Science Foundation (NSF) grant OISE-1743753, high-performance computing support from Cheyenne (doi:10.5065/D6RX99HX) provided by NCAR's Computational and Information Systems Laboratory, sponsored by NSF, and Blaž Gasparini and Maximilien Bolot for helpful discussions.

References

Atlas, R., Bretherton, C. S., Khairoutdinov, M. F., & Blossey, P. N. (2022). Hallett-mossop rime splintering dims cumulus clouds over the southern ocean: New insight from nudged global storm-resolving simulations. *AGU Advances*, *3*(2), e2021AV000454. doi: https://doi.org/10.1029/2021AV000454

Cazenave, Q., Ceccaldi, M., Delanoë, J., Pelon, J., Groß, S., & Heymsfield, A. (2019). Evolution of dardar-cloud ice cloud retrievals: new parameters and impacts on the retrieved microphysical properties. *Atmos. Meas. Tech.*, *12*(5), 2819-2835. (AMT) doi: 10.5194/amt-12-2819-2019

Cooper, W. A. (1986). Ice initiation in natural clouds. *Meteorological Monographs*, *21*(43), 29-32. doi: 10.1175/0065-9401-21.43.29

Delanoë, J., & Hogan, R. J. (2010). Combined cloudsat-calipso-modis retrievals of the properties of ice clouds. *Journal of Geophysical Research: Atmospheres*, *115*(D4). doi: https://doi.org/10.1029/2009JD012346

Deng, M., Mace, G. G., & Wang, Z. (2016). Anvil productivities of tropical deep convective clusters and their regional differences. *Journal of the Atmospheric Sciences*, *73*(9), 3467-3487. doi: 10.1175/jas-d-15-0239.1

Deng, M., Mace, G. G., Wang, Z., & Berry, E. (2015). Cloudsat 2c-ice product update with a new ze parameterization in lidar-only region. *Journal of Geophysical Research: Atmospheres*, *120*(23), 12,198-12,208. doi: https://doi.org/10.1002/2015JD023600

Doelling, D. R., Loeb, N. G., Keyes, D. F., Nordeen, M. L., Morstad, D., Nguyen, C., ... Sun, M. (2013). Geostationary enhanced temporal interpolation for ceres flux products. *Journal of Atmospheric and Oceanic Technology*, *30*(6),

1072-1090. doi: 10.1175/jtech-d-12-00136.1

Hartmann, D. L., Moy, L. A., & Fu, Q. (2001). Tropical convection and the energy balance at the top of the atmosphere. *Journal of Climate*, *14*(24), 4495-4511. doi: 10.1175/1520-0442(2001)014⟨4495:tcateb⟩2.0.co;2

Hersbach, H., Bell, B., Berrisford, P., Hirahara, S., Horányi, A., Muñoz-Sabater, J., ... Thépaut, J.-N. (2020). The era5 global reanalysis. *Quarterly Journal of the Royal Meteorological Society*, *146*(730), 1999-2049. doi: 10.1002/qj.3803

Hong, Y., Liu, G., & Li, J.-L. F. (2016). Assessing the radiative effects of global ice clouds based on cloudsat and calipso measurements. *Journal of Climate*, *29*(21), 7651-7674. doi: 10.1175/jcli-d-15-0799.1

Hu, Z., Lamraoui, F., & Kuang, Z. (2021). Influence of upper-troposphere stratification and cloud–radiation interaction on convective overshoots in the tropical tropopause layer. *Journal of the Atmospheric Sciences*, *78*(8), 2493-2509. doi: 10.1175/jas-d-20-0241.1

Jensen, E. J., Pfister, L., Jordan, D. E., Bui, T. V., Ueyama, R., Singh, H. B., ... Pfeilsticker, K. (2017). The nasa airborne tropical tropopause experiment high-altitude aircraft measurements in the tropical western pacific. *Bulletin of the American Meteorological Society*, *98*(1), 129-+. doi: 10.1175/bams-d-14-00263.1

Khairoutdinov, M. F., Blossey, P. N., & Bretherton, C. S. (2022). Global system for atmospheric modeling: Model description and preliminary results. *Earth and Space Science Open Archive*, 39. doi: doi:10.1002/essoar.10509977.1

Khairoutdinov, M. F., & Randall, D. A. (2003). Cloud resolving modeling of the arm summer 1997 iop: Model formulation, results, uncertainties, and sensitivities. *Journal of the Atmospheric Sciences*, *60*(4), 607-625. doi: 10.1175/1520-0469(2003)060⟨0607:crmota⟩2.0.co;2

Krämer, M., Rolf, C., & Spelten, N. (2020). *The cirrus guide ii in-situ aircraft data set.* doi: 10.34730/266ca2a41f4946ff97d874bfa458254c

Krämer, M., Rolf, C., Spelten, N., Afchine, A., Fahey, D., Jensen, E., ... Sourdeval, O. (2020). A microphysics guide to cirrus – part 2: Climatologies of clouds and humidity from observations. *Atmos. Chem. Phys.*, *20*(21), 12569-12608. (ACP) doi: 10.5194/acp-20-12569-2020

Morrison, H., Curry, J. A., & Khvorostyanov, V. I. (2005). A new double-moment

365 microphysics parameterization for application in cloud and climate models.
366 part i: Description. *Journal of the Atmospheric Sciences*, *62*(6), 1665-1677.
367 doi: 10.1175/jas3446.1

368 Morrison, H., & Milbrandt, J. A. (2015). Parameterization of cloud microphysics
369 based on the prediction of bulk ice particle properties. part i: Scheme descrip-
370 tion and idealized tests. *Journal of the Atmospheric Sciences*, *72*(1), 287-311.
371 doi: 10.1175/jas-d-14-0065.1

372 NASA/LARC/SD/ASDC. (2017). *Ceres and geo-enhanced toa, within-atmosphere*
373 *and surface fluxes, clouds and aerosols 1-hourly terra edition4a.* NASA Lang-
374 ley Atmospheric Science Data Center DAAC. doi: 10.5067/TERRA+AQUA/
375 CERES/SYN1DEG-1HOUR_L3.004A

376 Nugent, J. M., Turbeville, S. M., Bretherton, C. S., Blossey, P. N., & Ackerman,
377 T. P. (2022). Tropical cirrus in global storm-resolving models: 1. role
378 of deep convection. *Earth and Space Science*, *9*(2), e2021EA001965. doi:
379 https://doi.org/10.1029/2021EA001965

380 Pan, L. L., Atlas, E. L., Salawitch, R. J., Honomichl, S. B., Bresch, J. F., Randel,
381 W. J., ... Wolfe, G. (2017). The convective transport of active species in the
382 tropics (contrast) experiment. *Bulletin of the American Meteorological Society*,
383 *98*(1), 106-128. doi: 10.1175/bams-d-14-00272.1

384 Stanford, M. W., Varble, A., Zipser, E., Strapp, J. W., Leroy, D., Schwarzenboeck,
385 A., ... Protat, A. (2017). A ubiquitous ice size bias in simulations of trop-
386 ical deep convection. *Atmos. Chem. Phys.*, *17*(15), 9599-9621. (ACP) doi:
387 10.5194/acp-17-9599-2017

388 Sullivan, S. C., & Voigt, A. (2021). Ice microphysical processes exert a strong con-
389 trol on the simulated radiative energy budget in the tropics. *Communications*
390 *Earth & Environment*, *2*(1), 137. doi: 10.1038/s43247-021-00206-7

391 Thompson, G., Field, P. R., Rasmussen, R. M., & Hall, W. D. (2008). Explicit fore-
392 casts of winter precipitation using an improved bulk microphysics scheme. part
393 ii: Implementation of a new snow parameterization. *Monthly Weather Review*,
394 *136*(12), 5095-5115. doi: 10.1175/2008mwr2387.1

395 Toon, O. B., Starr, D. O., Jensen, E. J., Newman, P. A., Platnick, S., Schoe-
396 berl, M. R., ... Pickering, K. E. (2010). Planning, implementation, and
397 first results of the tropical composition, cloud and climate coupling experi-

ment (tc4). *Journal of Geophysical Research: Atmospheres*, *115*(D10). doi: https://doi.org/10.1029/2009JD013073

Turbeville, S. M., Nugent, J. M., Ackerman, T. P., Bretherton, C. S., & Blossey, P. N. (2022). Tropical cirrus in global storm-resolving models: 2. cirrus life cycle and top-of-atmosphere radiative fluxes. *Earth and Space Science*, *9*(2), e2021EA001978. doi: https://doi.org/10.1029/2021EA001978

Wendisch, M., Pöschl, U., Andreae, M. O., Machado, L. A. T., Albrecht, R., Schlager, H., ... Zöger, M. (2016). Acridicon–chuva campaign: Studying tropical deep convective clouds and precipitation over amazonia using the new german research aircraft halo. *Bulletin of the American Meteorological Society*, *97*(10), 1885-1908. doi: 10.1175/bams-d-14-00255.1

Figure 1.

Zonally averaged cloud radiative effects (CREs) and biases

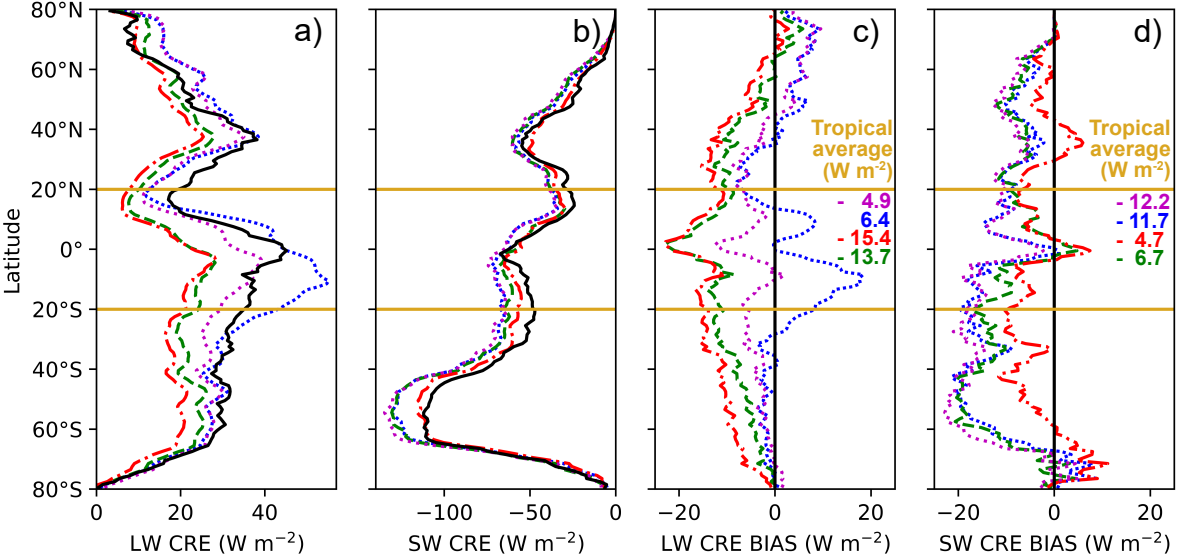

Observations

CERES

Simulations

P3 M2005 Thompson SAM1MOM

Figure 2.

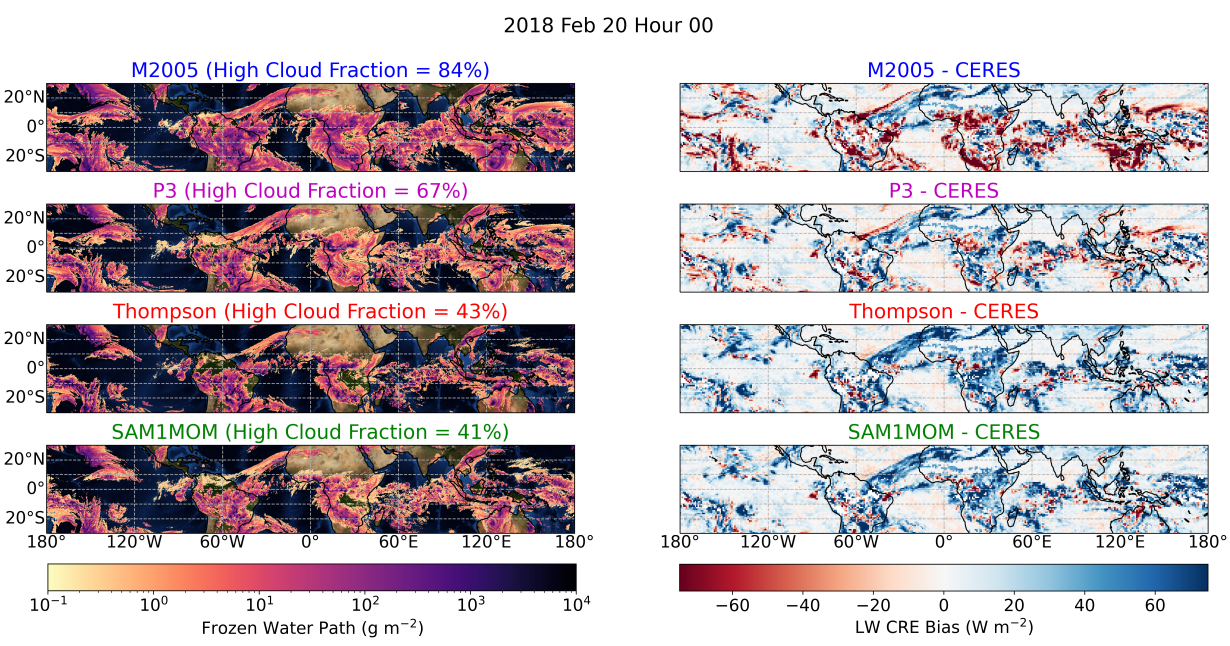
2018 Feb 20 Hour 00
M2005 (High Cloud Fraction = 84%)
P3 (High Cloud Fraction = 67%)
Thompson (High Cloud Fraction = 43%)
SAM1MOM (High Cloud Fraction = 41%)
M2005 - CERES
P3 - CERES
Thompson - CERES
SAM1MOM - CERES
20°N
0°
20°S
180°
120°W
60°W
0°
60°E
120°E
180°
10^{-1}
10^{0}
10^{1}
10^{2}
10^{3}
10^{4}
Frozen Water Path (g m^{-2})
−60
−40
−20
0
20
40
60
LW CRE Bias (W m^{-2})

Figure 3.

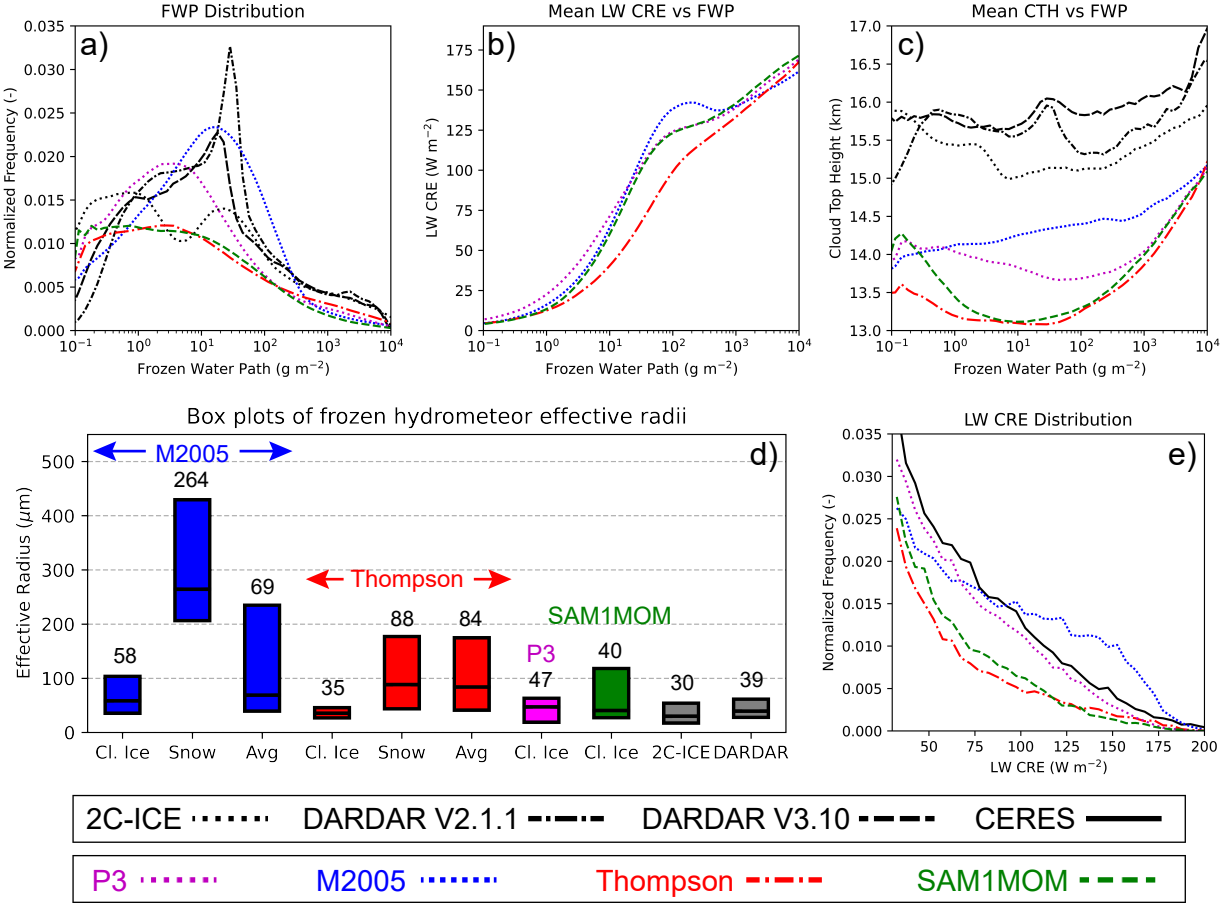
FWP Distribution
a)
Normalized Frequency (-)
Frozen Water Path (g m^{-2})
Mean LW CRE vs FWP
b)
LW CRE (W m^{-2})
Frozen Water Path (g m^{-2})
Mean CTH vs FWP
c)
Cloud Top Height (km)
Frozen Water Path (g m^{-2})
Box plots of frozen hydrometeor effective radii
d)
M2005
Thompson
SAM1MOM
Effective Radius (μm)
58
264
69
35
88
84
P3
47
40
30
39
Cl. Ice
Snow
Avg
Cl. Ice
Snow
Avg
Cl. Ice
Cl. Ice
2C-ICE
DARDAR
LW CRE Distribution
e)
Normalized Frequency (-)
LW CRE (W m^{-2})
2C-ICE
DARDAR V2.1.1
DARDAR V3.10
CERES
P3
M2005
Thompson
SAM1MOM

Figure 4.

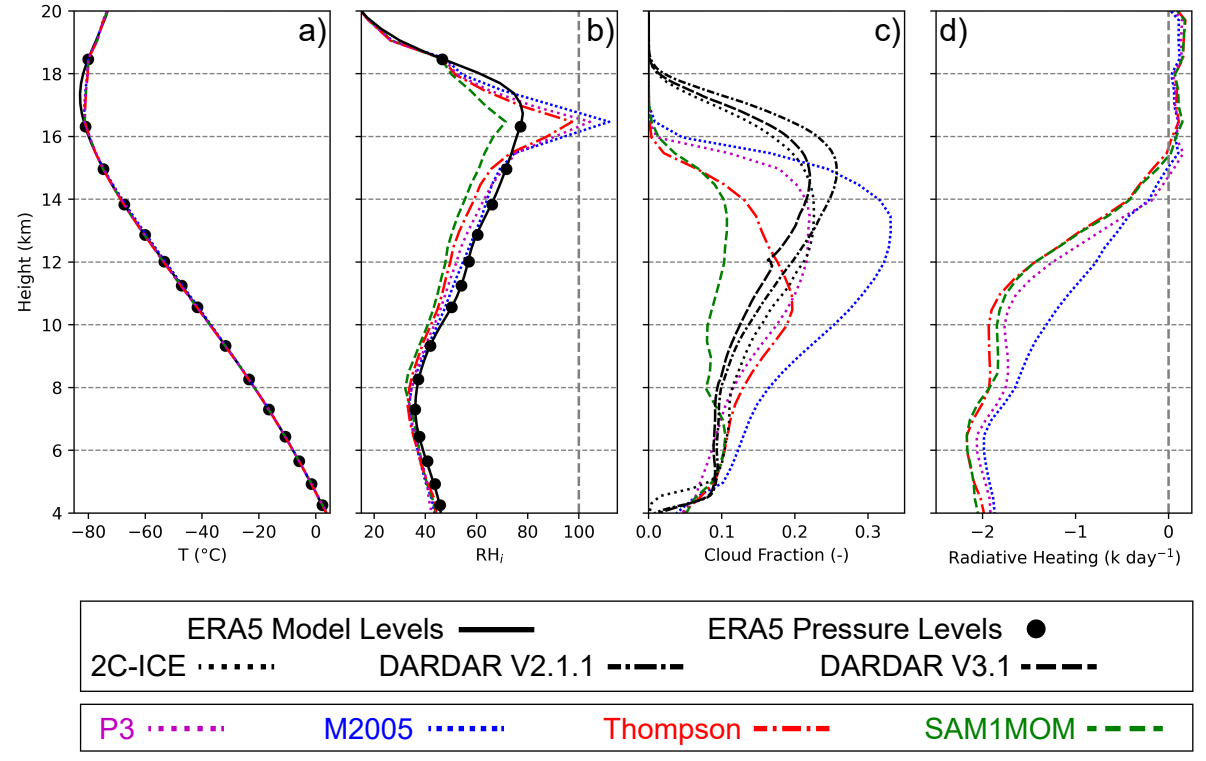
a)
b)
c)
d)
Height (km)
T (°C)
RH$_i$
Cloud Fraction (-)
Radiative Heating (k day^{-1})
ERA5 Model Levels
ERA5 Pressure Levels
2C-ICE
DARDAR V2.1.1
DARDAR V3.1
P3
M2005
Thompson
SAM1MOM

Figure 5.

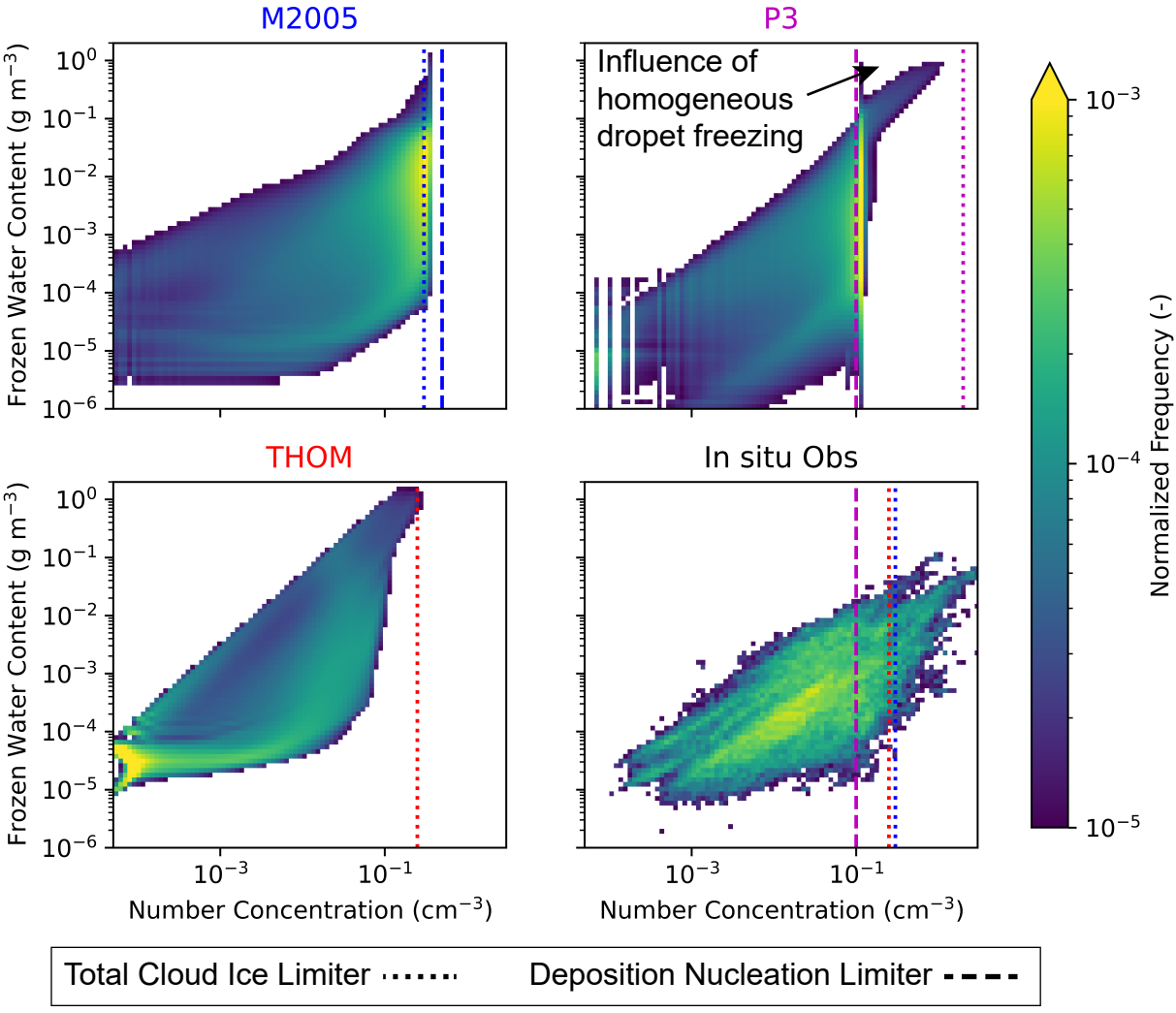
M2005
P3
THOM
In situ Obs
Influence of
homogeneous
dropet freezing
Frozen Water Content (g m^{-3})
Number Concentration (cm^{-3})
Normalized Frequency (-)
10^{0}
10^{-1}
10^{-2}
10^{-3}
10^{-4}
10^{-5}
10^{-6}
Total Cloud Ice Limiter
Deposition Nucleation Limiter